RSC Advances

ROYAL SOCIETY OF CHEMISTRY

www.rsc.org/advances

RSC Advances

ARTICLE

Received 00th January 20xx,

Accepted 00th January 20xx

DOI: 10.1039/x0xx00000x

www.rsc.org/

Functional quasi-solid-state electrolytes for dye sensitized solar cells prepared by amine alkylation reaction.

Andigoni Apostolopoulou[a,b], Antonis Margalias[a], Elias Stathatos[a,*]

Novel quasi-solid state electrolytes for dye-sensitized solar cells (QSS-DSCs) are prepared by the amine alkylation reaction. In particular two oligomers of poly(propylene oxide) and one block oligomer of poly(ethylene oxide)/poly(propylene oxide) with two amino groups grafted at both edges of the oligomers were used as amine sources while iodoethane as alkyl halide for substitution reactions. The nucleophilic aliphatic substitution (of the halide) reaction gives a higher substituted amine product and iodide ion which is essential for QSS-DSCs operation. Fourier transform infrared and UV-Vis spectroscopy, differential scanning calorimetry as well as electrochemical impedance spectroscopy were employed to characterize the resulting material after alkylation reaction. The sequential quasi-solid state electrolytes only containing the new quasi-solid materials after mixing amino ended oligomers with iodoethane and iodine without any plasticizer and additional iodide sources were examined as gel electrolytes in QSS-DSCs consisted of thin and transparent TiO_2 photoelectrodes sensitized with N-719 Ruthenium complex. The cells were found to be durable to thermal and light soaking exposure while a maximum overall efficiency of 3.7% was recorded without the presence of any solvent or additive for voltage and current enhancement.

Introduction

Almost twenty five years ago, dye-sensitized photoelectrochemical solar cells (DSCs) were proposed as alternative structures with competitive performance to amorphous silicon photovoltaic cells.[1-4] Simple fabrication process, transparency and relatively low cost were the main advantages over the conventional photovoltaics while new and smart applications employing DSCs continuously appear after the first demonstration of this technology.[5,6] Since then, the components of a DSC have more or less been established and they are: a TiO_2 nanocrystalline film deposited on a SnO_2:F transparent conductive electrode (negative electrode), a ruthenium bipyridyl derivative adsorbed and chemically anchored on TiO_2 films, an electrolyte bearing I^-/I_3^- redox mediator and a platinized SnO_2:F electrode (positive electrode). However, liquid electrolytes cause several problems to the cell fabrication steps. Leakage and volatilization issues of solvents in combination with poor long term stability of liquid based electrolytes put serious obstacles to the commercialization of DSCs.[7,8] In order to overcome the aforementioned problems several approaches have been proposed to replace liquid electrolytes with solid alternatives.[9] Somehow, the solid electrolytes should satisfy successful contact with TiO_2 particles at mesoporous electrode and enhanced values of conductivities.[10] A large number of published works is referred to the use of small molecules,[11] inorganic particles[12] and conducting polymers[13,14] as solid electrolytes in DSCs. Unfortunately, solar cells with solid electrolytes exhibit relatively low efficiencies because of high recombination rates at TiO_2/solid electrolyte interface besides the low conductivity of the solid electrolyte itself.[15] One main reason for this low performance is the imperfect wetting of porous TiO_2 film and lack of sufficient electric contact with working electrode by the solid-state electrolyte. Alternatively to the application of materials in solid state, many researchers have chosen to introduce gelifiers into the electrolyte, thus making the so-called quasi-solid state DSCs (QSS-DSCs).[16-18] QSS-DSCs have lower efficiency than liquid cells, mainly due to lower ionic conductivity, but efficiency values are still kept at satisfactory levels. This is usually due to the presence of solvents which are prevented from leaking and volatilizing by the presence of polymer or oligomer network with or without inorganic particles and fillers.[19] Quasi-solid state electrolytes are roughly distinguished into three categories: (1) Gel electrolyte can be formed after addition of organic or inorganic (or both) thickeners.[20] Such materials may be long-chain polymers like poly (ethylene oxide) or inorganic nanoparticles like titania or silica;[21] (2) By the in situ polymerization of a polymerizable precursor into the electrolyte solution;[22] (3) Finally, a third route is to produce a gel incorporating the I^-/I_3^- redox couple through the sol-gel process by using a sol-gel precursor, like a titanium or silicon alkoxide.[23,24] The basic advantage of the quasi-solid state over solid state electrolyte is that it is applied at an early stage of the preparation as it is still fluid, it penetrates into the titania nanoporous structure and ensures electrical conduction between titania nanocrystallites and electrolyte. However, the solar cell cannot be functioned without a sufficiently expanded organic subphase mainly due to reasonably good values for ionic conductivity which is made possible only through the organic subphase.

In the present work, we explore for first time the usage of novel quasi-solid state electrolytes prepared by the amine alkylation reaction in QSS-DSCs. In particular we explore the substitution reaction among two oligomers of poly(propylene oxide) and one block oligomer of poly(ethylene oxide)/poly(propylene oxide) with two amino groups grafted at both edges as amine sources with iodoethane as alkyl halide. The iodide ion as a product of the amine alkylation reaction is one of the main species for I^-/I_3^- redox mediator avoiding the use of expensive ionic liquids or/and inorganic iodide salts which are usually crystallized in the electrolyte diminishing the efficiency of the cells with time. The presence of poly(ethylene oxide)/or and poly(propylene oxide) chains are necessary as ionic conductive media for functional QSS-DSCs. Furthermore, the importance of the

[a] Department of Electrical Engineering, Technological-Educational Institute of Western Greece, GR-26334 Patras, Greece.
[b] Physics Dept., University of Patras, 26500 Patras, Greece.

*Corresponding author: Phone: +30 2610-369242, Fax: +30 2610-369193, e-mail: estathatos@teiwest.gr (prof. Elias Stathatos)

proposed method is that we do not use any solvent usually employed in QSS-DSCs eliminating the case of solvent leakage with time of operation or finally any additive for voltage and current improvement.

Experimental

Materials

For the electrolyte fabrication step, we used iodoethane (IoE, >99%, Aldrich), (Poly(propylene glycol) bis(2-aminopropyl ether) average molecular weight 230 (APPG 230, Aldrich), Poly(propylene glycol) bis(2-aminopropyl ether) average molecular weight 400 (APPG 400, Aldrich), O,O'-Bis(2-aminopropyl) polypropylene glycol-block-polyethylene glycol-block-polypropylene glycol 500 (Jeffamine ED-600, Aldrich), Iodine (>99.8%, Fisher Scientific) which were used as received. Titanium(IV) butoxide (TBO, 97%, Aldrich), Poly(ethylene glycol)-block-Poly(propylene glycol)-block-Poly(ethylene glycol) (MW≈5800, Pluronic P123, Aldrich), glacial acetic acid (AcOH, 99-100%, Aldrich) were used to make precursor TiO_2 sols. Chloroplatinic acid hexahydrate (H_2PtCl_6, reagent grade) and all solvents were of analytic grade and purchased from Sigma-Aldrich. *Cis*-diisothiocyanato-bis(2,2'-bipyridyl-4,4'-dicarboxylato) ruthenium(II) bis(tetrabutylammonium), N719 was purchased from Solaronix S.A, Switzerland. SnO_2:F transparent conductive electrodes (FTO, TEC^{TM} A8) 8 Ohm/square were purchased from Pilkington NSG Group.

Methods

FT-IR spectra for all electrolytes in gel morphology were monitored with a Jasco 4100 spectrophotometer (4000–350 cm^{-1}, resolution 0.7 cm^{-1}) by forming thin films on silicon wafers. The absorption spectra of the compounds in films were obtained using a Hitachi U-2900 UV-Vis spectrophotometer. The Differential Scanning Calorimetry-Thermogravimetric analysis (DSC-TGA) was performed for all electrolytes with a Perkin Elmer, STA6000 instrument. The transition temperature from gel to liquid state (T_{gel}) of the electrolyte was determined with DSC using 10-15 mg of each sample which were sealed in an aluminium pan and heated at a rate of 10 ^{o}C/min from room temperature to 160 ^{o}C.

For the *I-V* curves of the solar cells, the samples were illuminated with Xe light using a Solar Light Co. solar simulator (model 16S-300) equipped with AM 0 and AM 1.5 direct Air Mass filters to simulate solar radiation at the surface of the earth. The light intensity was kept constant at 1000 W/m^2 measured with a Newport power meter (843-R). Finally, the *I-V* curves were recorded by connecting the cells to a Keithley Source Meter (model 2601A) which was controlled by Keithley computer software (LabTracer). The cell active area was constant to 2 cm^2 while 0.3 cm^2 black mask was used in all measurements. Cell performance parameters, including short-circuit current density (J_{SC}), open circuit voltage (V_{OC}), maximum power (P_{max}), fill factor (*FF*) and overall cell conversion efficiency, were measured and calculated from each *J-V* characteristic curve. In each case, we made three devices which were tested under the same conditions in order to avoid any misleading estimation of their efficiency while the mean values of every measured parameter for each case appear in all presented Tables. Incident photon-to-current conversion efficiency (IPCE) was measured for all cells after illumination with Xe light source using a filter monochromator (IQE 200TM, Newport).

Complex impedance measurements were performed on square shaped samples with thickness of ~80 micrometers sandwiched between two copper electrodes of 1 cm^2 effective area. Besides, electrochemical Impedance Spectroscopy (EIS) characterization was carried out in dark and under illumination using the same Xe light source that was used for monitoring the *J-V* curves. EIS measurements were performed without the use of a mask with Metrohm Autolab 3.v potentiostat galvanostat (Model PGSTAT 128N) through a frequency range of 100 kHz-0.1 Hz using a perturbation of ±10 mV over the open circuit potential. Experimental data are presented by scattering symbols while lines represent the fitted plots obtained using Nova 1.10 software.

Preparation of the quasi-solid electrolytes

Gel electrolytes with APPG and jeffamine ED-600 oligomers were prepared by reacting constant quantity of poly(propylene glycol)bis(2-aminopropyl ether) of molecular mass 230/400 or O,O'-Bis(2-aminopropyl) polypropylene glycol-block-polyethylene glycol-block-polypropylene glycol 500 with various concentrations of iodoethane in a vessel. The molar ratio among oligomers and iodoethane was finally varied as follows: [oligomer]/[iodoethane]=1/3, 1/6, 1/9, 1/12. The colour of the sol after two hours of stirring was yellowish while it was colourless at the first mixture of the two ingredients (Scheme 1). This is a first proof for iodide ions release in the sol. In the above mixture and after two hours of continuous stirring variable concentrations of iodine were added but always keeping the molar ratio [iodoethane]/[I_2]=10/1. The mixture remained as a liquid for one additional hour after iodine addition before it finally turned to a gel at ambient conditions.

Scheme 1. NH_2–PEG_x–NH_2 / IoE mixture at early stage (left bottle) and after two hours of stirring (right bottle).

Fabrication and characterization of quasi-solid dye-sensitized cells

Preparation of TiO_2 photoanodes sensitized with dye N-719

TiO_2 thin films were deposited by following a modified procedure of a previously reported method.[25,26] Briefly, for 5.2 ml solution, 0.332 g of P123 were mixed with 4 ml of isopropanol (*i*-PrOH) followed by addition of 0.4 ml of glacial acetic acid and 0.37 ml of TBO under vigorous stirring. After a few minutes of stirring, pre-cleaned FTO glasses were spin-coated at 1200 rpm (SPS, Spin 150). The films were heated up to 500 ^{o}C for 30 minutes using 20 ^{o}C/min heating ramp rate. This process was repeated 15 times while the final thickness of the films was about 4 micrometers according to SEM cross sectional images. Finally, all the TiO_2 films were immersed in an ethanol/acetonitrile (1/1 v/v) solution of N719 overnight (the dye concentration was $5 \cdot 10^{-4}$ M) in order to sensitize the TiO_2 electrode in the visible range of light. Excessive dye

molecules that weren't adsorbed on the TiO_2 surface were removed by rinsing the sensitized films with acetonitrile.

Fabrication of the solar cells

For the solar cell application the electrolytes were stirred for almost three hours, one drop of each electrolyte was placed on the top of the TiO_2 electrode with adsorbed dye molecules and a slightly platinized FTO counter electrode was pushed by hand on the top. The platinized FTO glass was made by casting a few drops of an H_2PtCl_6 solution (5 mg/1 ml of ethanol) followed by heating at 500 ^oC for 10 minutes. The two electrodes were stuck together by the presence of the gel electrolyte, while any further treatment of cells regarding to sealing was not applied.

Results and discussion

One of the main problems in the operation of DSCs with time is the electrolyte. The electrolytes in liquid phase, as referred before, are not the choice of many research groups because of their leakage and difficulties in sealing of the cells. However, even in the case of quasi-solid electrolytes several solvents are routinely used as basic components. Moreover, inorganic iodide salts such as LiI are also necessary in order to create the necessary redox mediator or for conductivity enhancement of the electrolyte. This usually causes unexpected problems to the crystallization of the inorganic salts in the organic phase of the quasi-solid electrolytes reducing the cells' performance with time.[27,28] In this work we propose a new idea for the creation of iodide ions in the quasi-solid state electrolyte by amine alkylation reaction between an alkyl halide such as iodoethane and amine species which could be present for instance, at an oligomer with double amine ends (i.e NH_2–PEG_x–NH_2) as presented in the scheme 2. At this scheme for reasons of simplicity we present only one amine group at the one end of the oligomers where R is PEG_x in this case. This nucleophilic aliphatic substitution of the iodide may finally result to the necessary iodide species for the creation of I^-/I_3^- redox couple in combination with the coexistence of I_2 in the mixture. The amine N functions as the nucleophile and attacks the electrophilic C of the alkyl iodide displacing the iodide and creating the new C-N bond.[29]

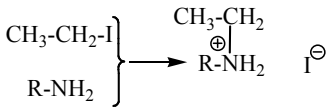

Scheme 2. Chemical reaction of an oligomer as amine source with iodoethane.

It is obvious that the resulting material with iodide counterion could have the same functionality with common ionic liquids with iodide counterion and inorganic iodide salts used in DSCs.

We examined the progress of the reaction in respect to Fourier transform infrared spectra (FTIR) for the three oligomers we used as amine sources. The results appear in Fig.1. The band at 2890 cm^{-1} arises from $–CH_2$- stretching vibrations and weak bands at ca. 1344 and 1471 cm^{-1} are ascribed to $–CH_2$- wagging vibrations which are characteristic of a molten and amorphous state of polyethylene glycol, while bands at about 1965 and 1801 cm^{-1} which could be characteristic vibrations of crystallized polyethylene glycol are finally not present. The initial evidence for the formation of the secondary amine is proved by the bands in the region between 1278 and 960 cm^{-1}, which are assigned to C-O vibrations while there is no evidence of a peak at 500 cm^{-1} refer to C-I stretching mode and it is characteristic for the iodoethane. Furthermore, N-H stretch occurs at 3500-3300 cm^{-1} and two bands appear for primary amines such as those exist at APPG 230/400 and ED-600. In case of the alkylation reaction a new peak at 3447 cm^{-1} appear which is characteristic for the creation of a secondary amine. Finally, N-H bending band at 1640-1560 cm^{-1} for primary amine is strongly perturbed after reaction which is finally a further evidence for the product described in scheme 2.[30]

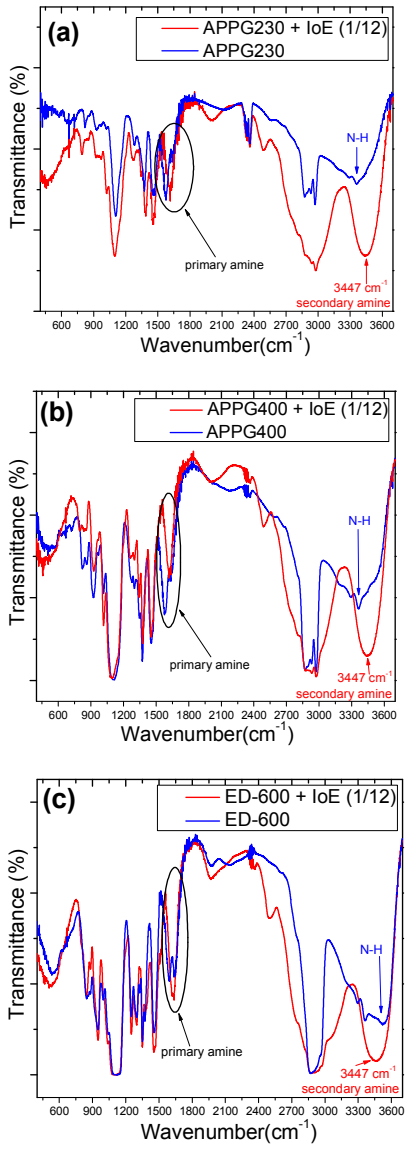

Figure 1. FTIR spectra of (a) APPG230 (b) APPG400 and (c) ED-600 before and after reaction with iodoethane.

In the above experiments the maximum quantity of iodoethane is used as a result of the better electrical performance achieved for the solar cells at this ratio and it will be shown to a next paragraph. The presence of iodide ions after the reaction of iodoethane with amine groups of the oligomers could be also spectroscopically proved. It is well known that co-presence of

iodine with iodide may form triiodide in an equilibrium reaction $I_2+I^- \rightarrow I_3^-$. The presence of triiodide ion in the electrolyte is very important for the functioning of the cell since it is the main ionic conductivity vehicle through the cathodic dark reaction $I_3^-+2e^- \rightarrow 3I^-$. The presence of triiodide could be spectroscopically determined by the peaks at 300 and 360 nm in the absorption spectrum of the electrolyte.[31] Indeed, measuring the absorbance of all prepared electrolytes with iodoethane and three different oligomers in the presence of iodine the peaks at the two wavelengths are obvious. As an example we present in Fig.2 the absorption spectrum of the electrolyte based on ED-600. However, the absorbance for the rest two oligomers is quite the same. As it can be seen the formation of the triiodide in the electrolyte is clear with two characteristic peaks located at 298 and 367 nm.

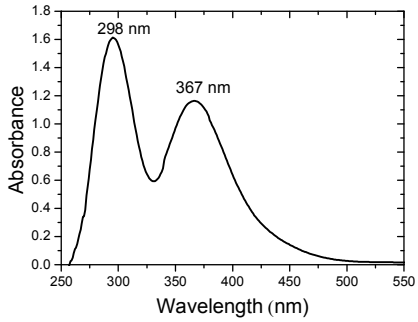

Figure 2. Absorption spectrum of triiodide in ED-600/iodoethane/I_2 electrolyte.

Differential scanning calorimetry was then used to determine the gel to liquid phase transition of the gel product of the scheme 2. T_{gel} from the gel to liquid state is very important since reflects the stability of the new electrolyte in the cell to the external temperature. In general, higher values for T_{gel} are useful in order to succeed long term stability of the solar cells. The obtained thermograms and the T_{gel} values for the three gels depending on the different oligomer used each time are presented in Figure 3. The phase transition temperature for all samples is ranged among 104 and 110 ^oC.

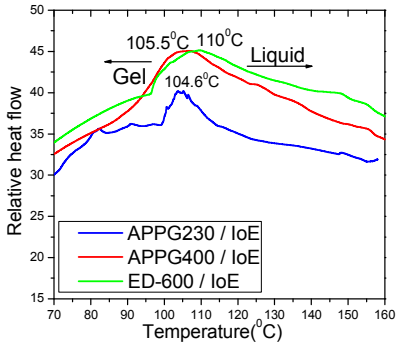

Figure 3. Differential scanning calorimetric thermograms of APPG230, APPG400 and ED-600 /iodoethane gels.

However, the small increase from 104.6 to 110 ^oC to the T_{gel} among the three samples can be explained by the difference of the oligomer chain length where an increased intermolecular interaction of carbon chain by van der Waals force could be happen. Additionally, the percentage of mass loss during the thermal treatment of the aforementioned samples appears in Fig.4. It is obvious that thermogravimetric analysis of the samples showed that there is a similar behaviour with that observed in thermograms of Fig.3 where a mass loss first appear for APPG230/iodoethane sample at relatively lower temperature than APPG400 and ED-600/iodoethane samples.

Ionic conductivity for the as-prepared electrolytes with three oligomers was calculated by examining the electrochemical properties of the materials. Figure 5 shows the complex impedance curves obtained for three electrolytes. All spectra contain two different regions: Incomplete semicircles in the high frequency and a spike in the low frequency. The semicircle part of the impedance spectra is related to ionic conduction of the bulk material.

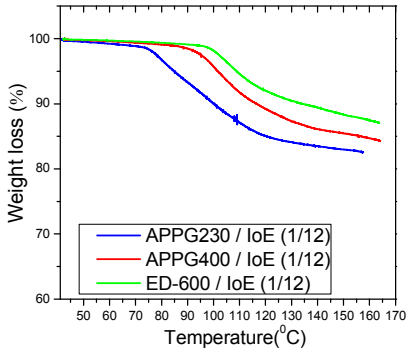

Figure 4. Thermogravimetric analysis of APPG230, APPG400 and ED-600 /iodoethane gels.

The presence of the semicircle is explained in terms of the equivalent circuit appear as an inset in Fig.5 by a parallel combination of a resistor (bulk resistance R_b) and a geometry capacitor (C_b). The resistor is referred to the migration of the ions in the volume of the organic matrix while the capacitor represents the immobile oligomers' chains. The use of symmetrical electrodes in the impedance analysis (the resistance of which is referred as R_e) allows the interface between electrolyte/electrode to be considered as capacitance.[32] The spike is represented by a Warburg impedance element (W).

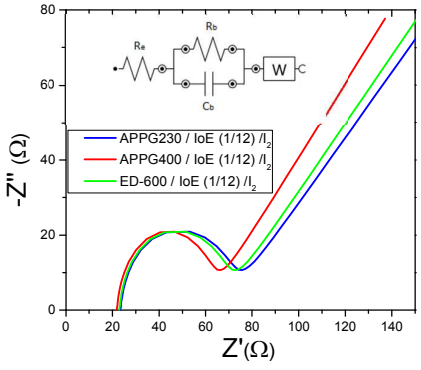

Figure 5. Complex impedance plot of APPG230, APPG400 and ED-600 /iodoethane/I_2 gels measured in dark.

The ionic conductivities (σ) for the three samples at room temperature were deduced according to the basic equation $\sigma = \frac{L}{R_b A}$ after fitting the data with equivalent circuit, where R_b is

the resistance appearing in parallel with the capacitor (C_b) in the inset image of Fig.5.[33] In the equation, L is the thickness of the gel electrolyte and A is the contact area between the two electrodes. The calculated values are presented in Table 1. The values for each of the three electrolytes seem to be very close but a relatively higher value was calculated for APPG400. However, the existence of a resistor connected in series (R_e) with the parallel system in the equivalent circuit presented in the inset of Fig.5 can be explained by the intersection of graphs with x-axis.

Table 1. Ionic conductivities of APPG230, APPG400 and ED-600 /iodoethane/ I_2 gels at room temperature.

Electrolyte	Conductivity ($\frac{S}{cm} \times 10^{-4}$)
APPG230 + IoE (1/12) / I_2	1.15
APPG400 + IoE (1/12) / I_2	1.37
ED-600 + IoE (1/12) / I_2	1.25

To further characterize the electron transport in the new electrolytes we studied the kinetic process at the TiO_2/dye electrode/electrolyte interfaces of DSCs using electrochemical impedance spectroscopy in the dark and appears in Fig.6a. In the dark, when a forward bias is applied to the cells, electrons transport through the TiO_2 electrode and primarily react with triiodide as iodide oxidized to triiodide ions at the counter electrode.[34,35] Experimental data obtained for the three electrolytes were fitted in terms of equivalent circuit which is depicted in Fig.6b. The order, in which each parallel combination of a resistance and the corresponding capacitance is appearing, is not always the same. To identify which resistance represents in each case depends on the values of each capacitance respectively. In Nyquist plot the first semicircle corresponds to the Pt/electrolyte interface, R_{pt}.[36]

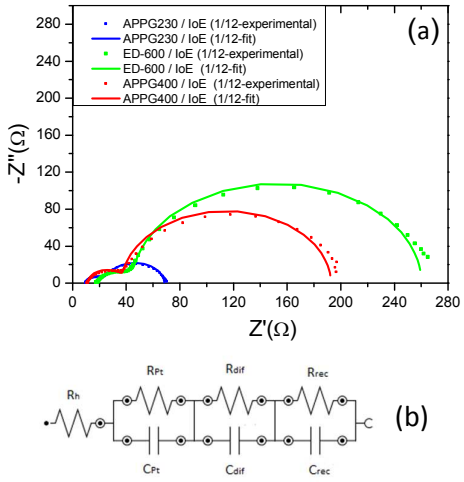

Figure 6. Nyquist plots (a) and the equivalent circuit (b) for the three electrolytes obtained from electrochemical impedance spectroscopy in the dark.

In particular, the charge transfer resistance at the counter electrode (R_{pt}) is represented as a semicircle in the impedance spectra. The resistance element related to the response in the intermediate frequency represents the charge transport at the TiO_2/dye/electrolyte interface (R_{rec}). The semicircle at the low frequency, which is attributed to the diffusion in the electrolyte (R_{dif}), was very small and not well formed indicating a fast diffusion. Finally, the intercept of the horizontal axis stands for the sheet resistance of the FTO substrate and the contact resistance of the FTO/TiO_2 (R_h). The total series resistance of the cell can be calculated using equation (1)

$$R_S = R_h + R_{pt} + R_{dif} \qquad \text{eq.1}$$

Furthermore, the R_{rec} resistance related to electron recombination processes occurring at the TiO_2-dye/electrolyte interfaces and C_{rec} (capacitance of the same interface) can be used to calculate the electron recombination lifetime at this interface according to the relation $\tau_n = R_{rec}C_{rec}$.[34] In general, the electron recombination at the TiO_2-dye/electrolyte interface is slightly lower when the values of R_{rec} and τ_n are larger. As it can be seen at Table 2 in the case of ED-600 the R_{rec} and τ_n values are the highest among the three electrolytes. This is probably due to the faster diffusion of triiodide ions in the electrolyte expecting better performance to the photovoltaic performance of the cells with this electrolyte. However, the chemical capacitance C_{rec} also corresponds to the trap energy distribution below the conduction band edge and it is related to the energy difference between E_F-$E_{F,redox}$ according to the equation 2:[35]

$$C_{rec} = C_o \exp\left(a \frac{E_F - E_{F,redox}}{K_B T}\right) \qquad \text{eq.2}$$

Table 2. Experimental results after fitting to the EIS data for DSCs based on the three electrolytes in dark.

Electrolyte	R_h (Ω)	R_{pt} (Ω)	C_{pt} (x10^{-4}F)	R_{rec} (Ω)	C_{rec} (x10^{-3}F)	R_s (Ω)	τ_n^* (msec)
APPG-230+ IoE (1/12)/I_2	9.7	9.4	0.32	43	0.71	25.6	31
APPG-400 + IoE (1/12)/I_2	11.2	26.1	0.27	155	0.55	37.3	85
ED-600 + IoE (1/12)/I_2	18.2	17.0	0.88	215	0.50	45.3	108

* *Calculated from EIS data*

E_F is the quasi Fermi level which determines the electron occupation of the trap and conduction band states while $E_{F,redox}$ is the energy difference between the quasi-Fermi level and the redox Fermi level, C_o is the pre-factor of the exponential, K_B is the Boltzmann constant and a=T/T_o where T_o is the characteristic temperature of the distribution and T is the temperature. Lower values for C_{rec} show an upward displacement of the TiO_2 conduction band edge. In our case the TiO_2 conduction band edge of the cells based on previous reasoning are finally more negative for the electrolytes based on ED-600 than the rest with APPG230 and APPG400 expecting a better behaviour to the open circuit voltage of the cells with ED-600 in the electrolyte.

The prepared redox electrolytes with oligomer/ iodoethane/I_2 were incorporated in solar cells using thin nanocrystalline TiO_2 films sensitized with N719 dye as photoanodes and their performances were monitored. The current density-voltage measurements for each oligomer/iodoethane ratio appear in Figure 7 obtained under 1 sun (AM 1.5G) illumination conditions while the

electrical parameters are presented in Table 3. It is obvious that the oligomer/iodoethane ratio equal to 1/12 is the more efficient to the performance of each solar cell we prepared. Increasing the quantity of iodoethane an increase to the performance is also observed for any of the three oligomers in the electrolyte. However, differences to the maximum overall performance among cells with different oligomer in the electrolyte are also evident. The obvious reason for this behaviour is the quantity of iodide ions in the electrolyte. The iodide ion leakage in the electrolyte is very critical to the overall performance of the cells so 12 times higher molar ratio than each oligomer finally creates the necessary concentration of iodoethane in the electrolyte. However, larger quantities of iodoethane in the electrolyte did not cause any additional improvement to the cells performance. The presence of ED-600 proved a better performance of the cells exhibiting an overall performance 3.7%.

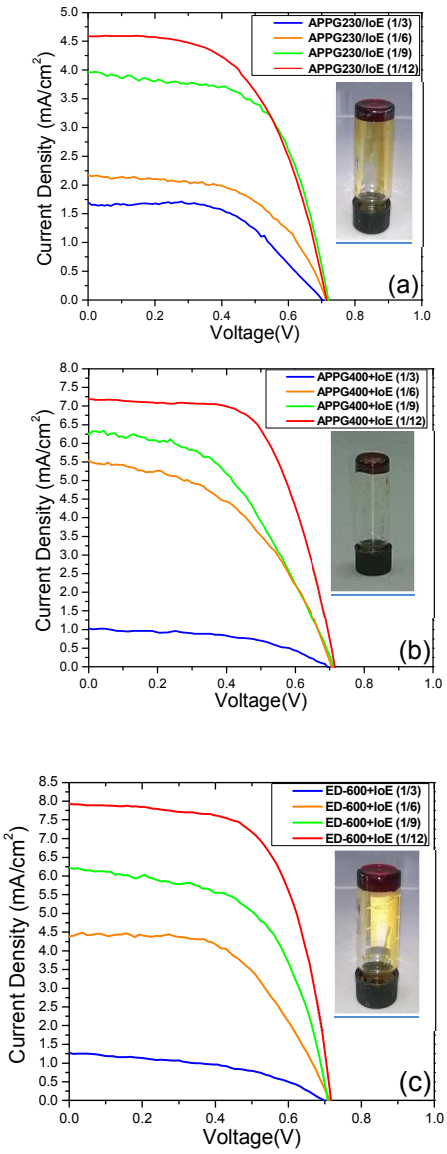

Figure 7. *J-V* curves of DSCs based on (a) APPG230 (b) APPG400 and (c) ED-600 and iodoethane.

The presence of APPG230 exhibited the worst performance among three electrolytes. This oligomer has also the shortest chain length among the three oligomers. It is worth noting that the open circuit voltage of all cells was around 0.7 volts which is a remarkable value in absence of any electrolyte additive for the voltage enhancement such as 4-tert-butylpyridine usually employed in DSC technology. The photocurrent action spectra for the cells with optimized electrolytes were also examined and presented on Fig.8. The maximum IPCE value of 65% at 512 nm obtained for the cell made with ED-600 oligomer while 53% was obtained for the case of APPG-230. These results are quite consistent with the current density values obtained for the cells. The dark current suppression was also examined to perceive the extent of the back electron transfer.

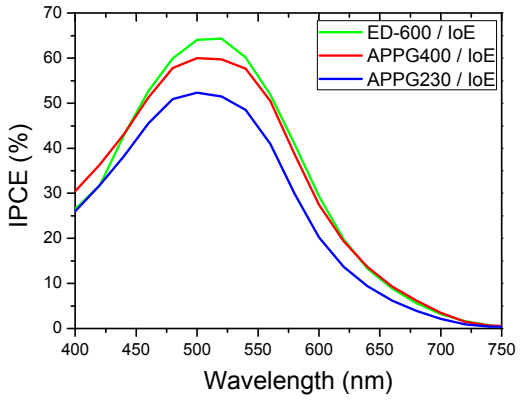

Figure 8. Photocurrent action spectra of DSCs based on (a) APPG230 (b) APPG400 (c) ED-600 and iodoethane.

Table 3. Comparison of the electrical properties of DSCs based on the three electrolytes in variable concentrations of iodoethane.

Electrolyte	V_{oc} (mV)	J_{sc} (mA/cm^2)	*FF*	n (%)
APPG230+ IoE (1/3)/I_2	700	1.7	0.56	0.7
APPG230+ IoE (1/6)/I_2	713	2.2	0.60	1.0
APPG230+ IoE (1/9)/I_2	714	4.0	0.60	1.7
APPG230+ IoE (1/12)/I_2	705	4.6	0.59	1.9
APPG400+ IoE (1/3)/I_2	690	1.1	0.60	0.5
APPG400+ IoE (1/6)/I_2	694	5.5	0.56	2.2
APPG400+ IoE (1/9)/I_2	702	6.3	0.58	2.6
APPG400+ IoE (1/12)/I_2	705	7.3	0.62	3.2
ED-600+ IoE (1/3)/I_2	695	1.3	0.48	0.5
ED-600+ IoE (1/6)/I_2	710	4.4	0.58	1.8
ED-600+ IoE (1/9)/I_2	706	6.3	0.55	2.5
ED-600+ IoE (1/12)/I_2	712	8.0	0.64	3.7

Fig.9 shows the dark current density in the cells made with the different electrolytes. The onset of the dark current for the DSCs fabricated with APPG230 and 400 electrolytes occurred at lower voltage compared with ED-600 which may be attributed to the slower

transport of triiodide ions from negative photoelectrode/electrolyte interface to the counter electrode.[37]

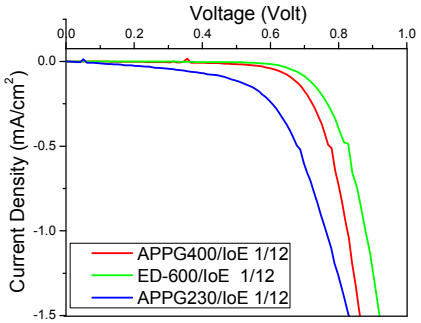

Figure 9. *J-V* curves of DSCs based on (a) APPG230 (b) APPG400 and (c) ED-600 and iodoethane in dark.

The effect on the electron transport of the interfaces in the DSCs under simulated solar light can be investigated with electrochemical impedance spectroscopy (EIS).

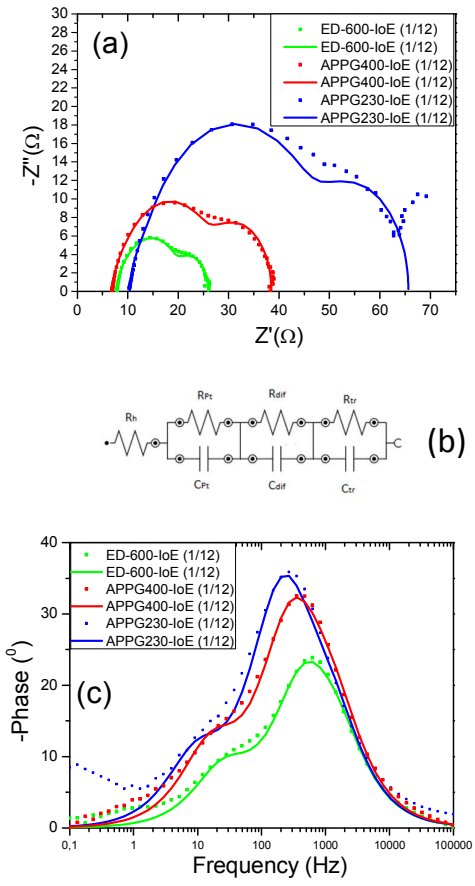

Figure 10. Nyquist diagram (a), equivalent circuit used for the fitting (b) and Bode diagram (c) for the three electrolytes obtained from electrochemical impedance spectroscopy under 1000 W/m^2 simulated solar light illumination.

Fig.10a shows the Nyquist while Fig.10c the Bode plot obtained from cells with optimized concentration of iodoethane. The charge transfer resistance at the counter electrode (R_{pt}) is represented as a semicircle in the impedance spectra and a peak in the Bode phase angle plot. The resistance element related to the response in the intermediate frequency represents the charge transport at the TiO_2/dye/electrolyte interface (R_{tr}) and shows diode like behaviour. The semicircle at the low frequency is attributed to the diffusion in the electrolyte (R_{dif}). The fitted parameters for the three cells are presented in Table 4 while the equivalent circuit which was used to fit the experimental data is presented in Figure 10b. J_{sc} values appear at Table 3 are in general qualitatively consistent with the R_{pt} and R_{tr} values of these cells at Table 4. Two factors that limit the short-circuit photocurrent are the efficiency of collecting the injected electrons at the transparent back contact and the catalytic ability of the counter electrode for the reduction of I_3^- ions to I^- ions.[38] If R_{tr} is low the efficiency of collecting the injected electrons at the transparent back contact increases, which results in an increase to the rate of electron transfer in the circuit and thereby the short circuit photocurrent of the pertinent DSC. Besides, if R_{pt} is also low, the rate of reduction of I_3^- ions and creation of I^- ions increases resulting an increase to the rate of regeneration of oxidized dye, the injection of electrons from the regenerated dye and thereby the J_{sc}. Finally, R_{dif} concerning the diffusion rate of I_3^- and I^- ions in the gel electrolyte is also consistent to J_{sc}. Smaller measured values for R_{dif} has beneficial effect to the J_{sc} and overall efficiency values. The mid-frequency shift to lower values in the Bode diagram may corresponds to an increase of the electron lifetime for APPG230 based electrolyte. Indeed, the electron lifetime can be determined by equation $\tau_n=R_{tr}C_{tr}$ where R_{tr} and C_{tr} are the resistance and capacitance of the TiO_2/dye/electrolyte interface.[39,40] The values for electron lifetime calculated from the above equation are presented in Table 4. It is then obvious that in the case of the APPG230 electrolyte an increase to the electron lifetime is measured which means a more effective suppression of the back reaction of the injected electrons with I_3^- in the electrolyte. However, the obtained values for each case are comparable. The low and high frequency peaks observed in the Bode plots correspond to triiodide diffusion in the electrolyte and charge transfer at the counter electrode, respectively. There are no significant changes of low and high frequency peaks implying that no unexpected reactions within the electrolyte and the counter electrode happened for the three electrolytes.

Table 4. Experimental results after fitting to the EIS data for DSCs based on the three electrolytes under simulated solar light.

Electrolyte	R_{pt} (Ω)	C_{pt} (x10^{-4}F)	R_{tr} (Ω)	C_{tr} (x10^{-4}F)	R_{dif} (Ω)	C_{dif} (x10^{-3}F)	R_s (Ω)	τ_n^* (msec)
APPG230+ IoE(1/12	33	0.40	3.5	0.42	18.7	1.1	62.2	0.15
APPG400+ IoE (1/12)	17	0.51	2.3	0.61	12.2	1.0	36.4	0.14
ED600+ IoE (1/12)	10	0.51	2.1	0.61	6.2	1.2	24.1	0.13

* *Calculated from EIS data*

Conclusions

For the first time a novel quasi-solid state electrolyte for dye sensitized solar cells is prepared through amine alkylation reaction. Two oligomers of poly(propylene oxide) (APPG230/400) and one block oligomer of poly(ethylene oxide)/poly(propylene oxide) (ED-600) as amine sources reacted with iodoethane resulting a gel material and iodide as counter ion. The new quasi-solid materials were thermally stable up to 110 ^{o}C which is advantageous for their long term stability. The use of different oligomers for the alkylation reaction showed also differences to the electron recombination and conduction band shift to the TiO_2 photoelectrodes after examination with EIS in dark. The as-presented electrolytes which finally do not contain any plasticizers, solvents or other additives were applied in DSCs where competitive efficiencies were obtained with a 3.7% maximum overall efficiency recorded in the case of ED-600. The higher value for overall efficiency can be attributed to the lower value of in series resistance of the cells besides the lower values of R_{tr} and R_{pt} measured with EIS under 1000 Wm^{-2} illumination.

Acknowledgements

The authors would like to acknowledge financial support for the present work from "Grant no. 11-ΣΥΝ-7-298, COOPERATION 2011" - Partnerships of Production and Research Institutions in Focused Research and Technology Sectors co-financed by the European Fund regional Development Fund (ERDF) of the European Union and National Resources.

Notes and references

1. A. Hagfeldt, G. Boschloo, L. Sun, L. Kloo, H. Pettersson, Chem. Reviews, 2010, **110**, 6595.

2. M. Grätzel, J. Photochem. Photobiol. C**,** 2003, **4**, 145.

3. N. Sharifi, F. Tajabadi, N. Taghavinia, Chem. Phys. Chem., 2014, **15**, 3902.

4. A. Jena, S. P. Mohanty, P. Kumar, J. Naduvath, V. Gondane, P. Lekha, J. Das, H. K. Narula, S. Mallick, P. Bhargava, Tran. of the Indian Ceramic Soc.**,** 2012, **71**, 1.

5. U. Mehmood, S. Rahman, K. Harrabi, I. A. Hussein, B. V. S. Reddy, Adv. in Mater. Sci. and Engineering**,** 2014, 974782.

6. Z. Lan, J. Wu, Progress in Chem.**,** 2010, **22**, 2248.

7. S. Y. Shen, R. X. Dong, P. T. Shih, V. Ramamurthy, J. J. Lin, K. C. Ho, ACS Appl. Mater. Interfaces, 2014, **6**, 18489.

8. S. Lee, Y. Jeon, Y. Lim, Md. A. Hossain, S. Lee, Y. Cho, H. Ju, W. Kim, Electrochimica Acta**,** 2013, **107**, 675.

9. J. Wu, Z. Lan, J. Lin, M. Huang, Y. Huang, L. Fan, G. Luo, ACS Chem. Rev. 2015, **115**, 2136.

10. C. Wu, L. Jia, S. Guo, S. Han, B. Chi, J. Pu, L. Jian, ACS Appl. Mater. Interfaces**,** 2013, **5**, 7886.

11. P. Wang, S. M. Zakeeruddin, P. Comte, I. Exnar, M. Grätzel, J. Am. Chem. Soc., 2003, **125**, 1166.

12. A. Konno, G. R. A. Kumara, R. Hata, K. Tennakone, Electrochemistry**,** 2002, **70**, 432.

13. J. Shi, L. Wang, Y. Liang, S. Peng, F. Cheng, J. Chen, The J. of Phys. Chem. C**,** 2010, **114**, 6814.

14. L. Jin, Z. Wu, T. Wei, J. Zhai, X. Zhang, Chem. Commun., 2011, **47**, 997.

15. M. N. Amalina, M. R. Mahmood, Adv. Mater. Research**,** 2013, **667**, 317.

16. T. M. W. J. Bandara, W. J. M. J. S. R. Jayasundara, M. A. K. L. Dissanayake, H. D. N. S. Fernado, M. Furlani, I. Albinsson, B-E. Mellander, Int. J. of Hydrogen Energy**,** 2014, **39**, 2997.

17. M. A. K. L. Dissanayake, R. Jayathissa, V. A. Senevirante, C. A. Thotawatthage, G. K. R. Senadeera, B-E. Mellander, Solid State Ionics**,** 2014, **265**, 85.

18. N. Manfredi, A. Bianchi, V. Causin, R. Ruffo, R. Simonutti, A. Abbotto, J. of Polymer Sc. Part A: Pol. Chem., 2014, **52**, 719.

19. S. Ibrahim, S. M. M. Yasin, N. M. Nee, R. Ahmad, M. R. Johan, J. of Non-Crystalline Solids**,** 2012, **358**, 210.

20. O. A. Ileperuma, Materials Technology, 2013, **28**, 65.

21. Y. Huang, W. Xiang, X. Zhou, S. Fang, Y. Lin, Electrochimica Acta**,** 2013, **89**, 29.

22. S.-H. Park, J. Lim, I.Y. Song, T. Lee Park, Adv. En. Mater.**,** 2014, **18**, DOI: 10.1002/aenm.201300489.

23. E. Stathatos, P. Lianos, U. Lavrencic-Stangar, B. Orel, Adv. Mater., 2002, **14**, 354.

24. E. Stathatos, P. Lianos, C. Krontiras, J. Phys. Chem. B.**,** 2001, **105**, 3486.

25. E. Stathatos, P. Lianos, C. Tsakiroglou, Microp. and Mesopor. Materials**,** 2004, **75**, 255.

26. T. Makris, V. Dracopoulos, T. Stergiopoulos, P. Lianos, Electrochimica Acta**,** 2011, ***56***, 2004.

27. E. Stathatos, P. Lianos, A. S. Vuk, B. Orel, Adv. Funct. Mater.**,** 2004, **14**, 45.

28. B. Orel, A. S. Vuk, R. Jese, P. Lianos, E. Stathatos, P. Judeinstein, Ph. Colomban, Solid State Ionics**,** 2003, **165**, 235.

29. March, Jerry, (1985) New York: Wiley, ISBN 0-471-85472-7.

30. J. Mijovic, S. Andjelic, Macromolecules**,** 1995, **28**, 2787.

31. V. Jovanovski, B. Orel, R. Jese, A. S. Vuk, G. Mali, S. B. Hocevar, J. Grdadolnik, E. Stathatos, P. Lianos, J. Phys. Chem. B**,** 2005, **109**, 14387.

32. N. N. Mobarak, A. Ahmad, M. P. Abdullah, N. Ramali, M. Y. A. Rahman, Electrochimica Acta**,** 2013, **92**, 161.

33. X. Qian, N. Gu, Z. Cheng, X. Yang, E. Wang, S. Dong, J. Solid State Electrochem, 2001, **6**, 8.

34. J. Bisquert, Phys. Chem. Chem. Phys.**,** 2003, **5**, 5360.

35. L. Tao, Z. Huo, S. Dai, Y. Ding, J. Zhu, C. Zhang, B. Zhang, J. Yao, M. K. Nazeeruddin, M. Grätzel, J. Phys. Chem. C**,** 2014, **118**, 16718.

36. K. Xia, Z. Peng, Z. Hu, J. Zhang, Z. Hu, Y. Zhu, Electrochimica Acta**,** 2015, **153**, 28.

37. L. Tao, Z. Huo, S. Dai, J. Zhu, C. Zhang, Y. Huang, B. Zhang, J. Yao, J. of Power Sources**,** 2014, **262**, 444.

38. S-Y. Shen, R-X. Dong, P-T. Shih, V. Ramamurthy, J-J. Lin, K-C. Ho, ACS Appl. Mater. Interfaces, 2014, **6**, 18489.

39. J. Bisquert, F. Fabregat-Santiago, I. Mora-Sero, G. Garcia-Belmonte, S. Gimenez, J. Phys. Chem. C 2009, **113**, 17278

40. H. Chen, L. Zhu, H. Liu, W. Li, Electrochimica Acta, 2013, **105**, 289.